# РОБОТЫ, МЕХАТРОНИКА И РОБОТОТЕХНИЧЕСКИЕ СИСТЕМЫ

DOI: 10.17587/mau.20.280-290

M. Yu. Rachkov, michyur@gmail.com, Moscow Politech

Corresponding author: Rachkov Mikhail Yu., D. Sc., Prof., Moscow Politech, Moscow, 107023, Russian Federation, e-mail: michyur@gmail.com

Accepted Desember 28, 2018

# **Modelling of Demining Manipulator Optimal Functioning**

#### Abstract

The paper describes the modelling of a demining manipulator that contains a pneumatic drive, an infrared mine detector and a mine neutralizator. The infrared mine detector identifies the mine position in the scanning mode of the manipulator and gives a control signal to an input of a manipulator drive control unit for accurate positioning of the neutralizator above the detected mine. A problem of the optimal manipulator positioning in the sense of the control energy consumption minimization is solved. The feedback loop contains only one sensor to perform the optimal positioning of the third-order control object due to an observer application. Modelling results of the infrared detector mine searching and of the neutralizator positioning by means of a pneumatic manipulator are presented. A comparison of modelling and experimental results shows that modelling assumptions correspond enough to real process parameters.

**Keywords:** modelling, demining manipulator, pneumatic drive, optimal positioning, infrared mine detector, observer

For citation:

Rachkov M. Yu. Modelling of Demining Manipulator Optimal Functioning, *Mekhatronika, Avtomatizatsia, Upravlenie*, 2019, vol. 20, no. 5, pp. 280—290.

УДК 004.896:621.865 DOI: 10.17587/mau.20.280-290

**М. Ю. Рачков,** д-р техн. наук, проф., michyur@gmail.com, Московский Политех

# Моделирование оптимального режима работы манипулятора для разминирования

Описывается моделирование манипулятора для разминирования, который содержит пневматический привод, инфракрасный датчик и нейтрализатор мин. Инфракрасный датчик определяет положение мины в режиме сканирования манипулятора и подает управляющий сигнал на вход блока управления привода манипулятора для точного позиционирования нейтрализатора над обнаруженной миной. Решена задача оптимального позиционирования манипулятора в смысле минимизации энергопотребления на управление. Контур обратной связи содержит только один датчик для выполнения оптимального позиционирования системы благодаря применению наблюдателя. Управление системой осуществляется с помощью пневматического сигнала. Информация о текущем состоянии системы подается от датчика давления, подключенного к пневматическим цилиндрам, и от наблюдателя. Представлена реализация системы оптимального управления, которая требует только трех блоков масштабирования и одного сумматора, при этом модель манипулятора состоит из двух интеграторов, одного сумматора и двух блоков масштабирования. Реализовано компьютерное моделирование работы инфракрасного датчика мин. Рассчитано затухание микроволн и потребляемая мошность на заданной глубине залегания мины в грунте. Работа инфракрасного датчика моделируется в двухфазном режиме поиска мин. Полученное распределение температуры внутри объема грунта, содержащего мину, после воздействия на рабочую зону микроволнами, позволяет получать информацию о местонахождении мины. Представлены результаты моделирования поиска мины инфракрасным датчиком и моделирования позиционирования нейтрализатора с помощью пневматического манипулятора. Сравнение результатов моделирования и эксперимента показывает, что допущения, принятые при моделировании, достаточно точно соответствуют параметрам реального процесса.

**Ключевые слова**: моделирование, манипулятор, разминирование, пневматический привод, оптимальное позиционирование, инфракрасный датчик, наблюдатель

#### Introduction

Landmines affect almost every aspect of life in states recovering from conflict. According to the UN Mine Action Service, there are more than 110 million mines spread across 68 countries [1]. The Convention on the Prohibition of the Use, Stockpiling, Production and Transfer of Anti-Personnel Mines and on their Destruction, known informally as Mine Ban Treaty, aims at eliminating anti-personnel landmines (AP-mines) around the world. To date, there are 164 state parties to the treaty.

If the cost of the mine removing would be about the cost of the mine, the main advantages of using the mine would disappear. Automation of demining operations can carry out this task with substantially reduced costs due to the special design of the demining system [2—6].

Automation of demining can be performed by means of autonomous robots equipped with a mine detection block and a mine neutralizator. A robot manipulator carries out searching trajectories of the detection block and positioning of the mine neutralizator.

For autonomous robots high payload-to-weight ratio of the manipulator is important. Pneumatic manipulators have such a possibility, compared to electric driven manipulators. Another desirable characteristic for autonomous systems is the minimization of the energy consumption of the onboard supply unit. This demands applying an optimal feedback control of the manipulator motion.

It was concluded in [7] that the third-order control provides a practical choice for effective control of pneumatic manipulators. Sometimes, in practice, it is impossible to measure a full phase vector because of design parameters of the manipulator. Minimizing the sensors number used for optimal control is important in this case.

The demining manipulator should fulfill the searching motion of the mine detector and the positioning of the demining equipment. Modelling of the infrared (IR) detector mine searching and of the mine neutralizator positioning by means of the pneumatic manipulator is presented.

## 1. System description

The demining system consists of the manipulator that is installed on a mobile robot (Fig. 1.1). The end-effector of the manipulator contains a mine detector and a mine neutralizator.

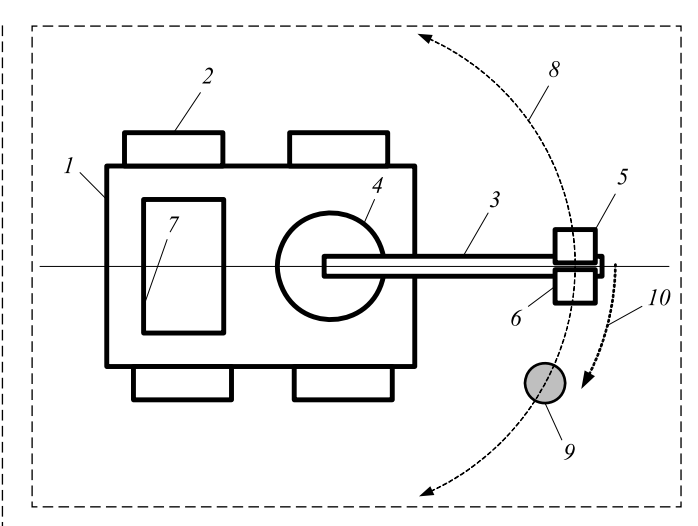


Fig. 1.1. General diagram of the system:

1- mobile robot; 2- wheels; 3- manipulator; 4- manipulator drive; 5- mine detector; 6- mine neutralizator; 7- control and supply block; 8- scanning trajectory; 9- mine; 10- neutralizator positioning trajectory

The mine detector performs scanning trajectories by means of the manipulator during robot motion across a minefield. After a mine is detected, the manipulator should perform the neutralizator positioning trajectory to place it over the detected mine.

The neutralizator is based on laser heating of the mine until the explosive filler ignites and starts to burn. If the mine has a metal case, the heat is conducted through the case and target irradiation is continued until the temperature of the inside wall and the temperature of the explosive filler exceeds its combustion temperature [8]. If it is a plastic case, the case is irradiated until it has been penetrated and the explosive filler is ignited, either directly from the laser radiation or from the flames burning the plastic case.

A functional diagram of the system is shown in Fig. 1.2.

The mine detector provides information about the mine angle position in the scanning mode of the manipulator. This information goes by a feedback loop to the control unit and changes the scanning mode

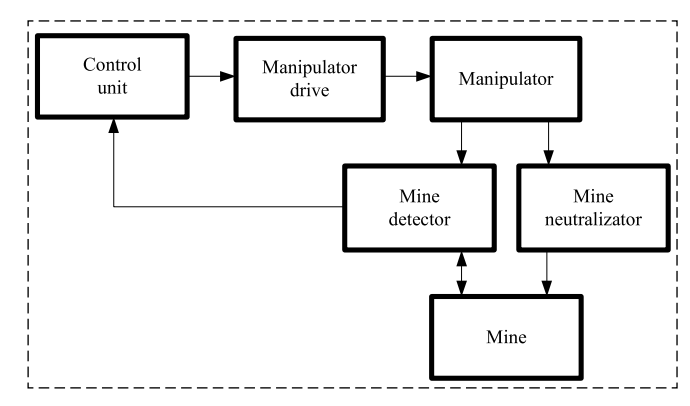


Fig. 1.2. Functional diagram of the system

with 180° rotation to the neutralizator positioning mode with rotation to the detected area. The manipulator drive performs positioning of the neutralizator according to the given angle. The angle is measured relatively to the central axis of the manipulator taking into account the design parameters of the neutralizator and its connection to the manipulator.

### 2. Mine detector modelling

The mine sensing is based on an infrared image analysis obtained during microwave soil heating and posterior cooling. The detector prototype contains a microwave klystron emitting 1 kW power at the frequency of 2.45 GHz and two infrared sensors sensitive in the range of 8—14 µm. Depending on the soil dielectric properties, the emitted radiation will be absorbed, reflected or transmitted through. Common plastic materials are transmissive, metals reflect the microwaves, and wet soil absorbs and converts the radiation to heat. Using this sensor, it is possible to image thermal gradients in the soil surface and detect different rates of temperature changes depending on the soil content [9].

The mine detector uses temperature gradients sensed over a homogeneous soil surface containing a plastic mine. According to the electromagnetic theory, a plane wave propagating in a lossy dielectric can be expressed by [10]:

$$E = E_0 e^{-\gamma z} = E_0 e^{-\alpha z} e^{-j\beta z}, \qquad (2.1)$$

where z is the propagation direction,  $E_0$  is the electric field in position z = 0, and  $\alpha$  and  $\beta$  are attenuation and phase constants for the material in which the wave is propagating. The propagation constant  $\gamma$ can be expressed by the following equation

$$\gamma = \sqrt{j\omega\mu(\sigma + j\omega\varepsilon)},\tag{2.2}$$

where  $\varepsilon = \varepsilon_r \varepsilon_0$  and  $\mu = \mu_r \mu_0$  are the dielectric permittivity and the magnetic permeability of the material expressed here relatively to the permittivity  $\varepsilon_0$ and permeability  $\mu_0$  in free space,  $\sigma$  is the material conductivity and  $\omega$  is the angular frequency of the wave. If  $\sigma$  is much bigger then  $\omega \varepsilon$ , the medium can be considered as a perfect conductor, if  $\sigma$  is much smaller then  $\omega\epsilon$  the medium can be considered as a perfect dielectric.

When a planar electromagnetic wave propagates into a soil surface, part of it will be refracted into the soil and the other part will be reflected to the air (Fig. 2.1).

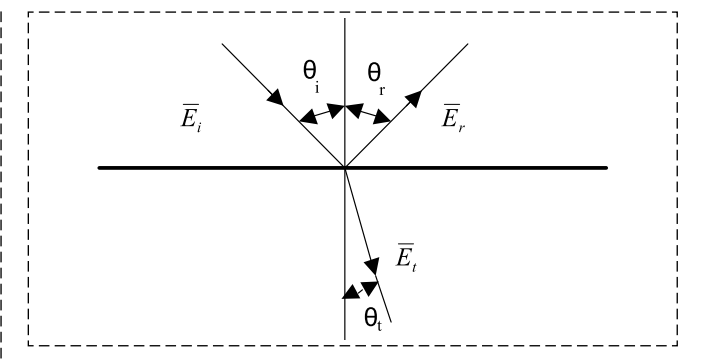


Fig. 2.1. Electromagnetic wave reflection and refraction

According to the Snell's law, reflection and refraction angles can be expressed by the following equations:

$$\theta_i = \theta_{ri} \tag{2.3}$$

$$\theta_i = \theta_r; \qquad (2.3)$$

$$\frac{\sin \theta_i}{\sin \theta_t} = n, \qquad (2.4)$$

where  $\theta_i$ ,  $\theta_r$  and  $\theta_t$  are incident, reflection and refraction angles respectively, n — refraction coefficient.

The ratio between the reflected  $(E_r)$  and the incident electric field  $(E_i)$  is the reflection coefficient. Depending on the type of wave polarization used (horizontal or vertical), this ratio can be expressed by  $R_h$  or  $R_v$ :

$$R_h = \frac{E_r}{E_i} = \frac{\cos \theta_i - \sqrt{\varepsilon_r - \sin^2 \theta_i}}{\cos \theta_i + \sqrt{\varepsilon_r - \sin^2 \theta_i}}; \qquad (2.5)$$

$$R_{v} = \frac{E_{r}}{E_{i}} = \frac{\varepsilon_{r} \cos \theta_{i} - \sqrt{\varepsilon_{r} - \sin^{2} \theta_{i}}}{\varepsilon_{r} \cos \theta_{i} + \sqrt{\varepsilon_{r} - \sin^{2} \theta_{i}}}.$$
 (2.6)

These expressions are useful to determine optimum incident angle in order to maximize the energy propagated into the second medium. The electric field can be related with the transmitted power using the Poynting vector expression and Maxwell laws [11]. In the far field, the electromagnetic power P can be expressed by:

$$P = \frac{1}{2n} |E|^2 A, \text{ [W]}$$
 (2.7)

where  $\eta$  is the impedance seen by the wave ( $\eta$  = =  $120\pi$  in free space) and A is the soil area enclosed by the valve radiation (in our case  $A = 0.1225 \text{ m}^2$ ). The heat generated in an elemental volume of material by a microwave electric field depends mainly on the frequency and on the dielectric properties of the material [12]. The power  $P_{\nu}$  absorbed per unit of volume can be calculated through the following equation,

$$Pv = \omega E^2 \epsilon \tan \delta$$
, [W/m<sup>3</sup>] (2.8)

where  $\omega$  is the angular frequency, E is the absolute value of the electrical field,  $\varepsilon$  is the material permittivity, and  $\tan(\delta)$  is the tangent of losses in the medium that can be expressed by the following equation [13]:

$$\tan \delta = \frac{\omega \varepsilon'' + \sigma}{\omega \varepsilon'}, \qquad (2.9)$$

where  $\epsilon'$  and  $\epsilon''$  are real and complex parts of the permittivity

$$\varepsilon = \varepsilon' + j\varepsilon'' = \varepsilon' (1 - j \tan \delta). \tag{2.10}$$

A computational implementation of the model was done by Matlab [14]. It calculates the microwave attenuation and the power absorbed from the valve output, above the ground, up to a specified depth in the ground. Vertical polarity is used by default in the implementation. The user can choose to visualize the power or the electrical field and can model the soil with or without a mine. It is also possible to visualize

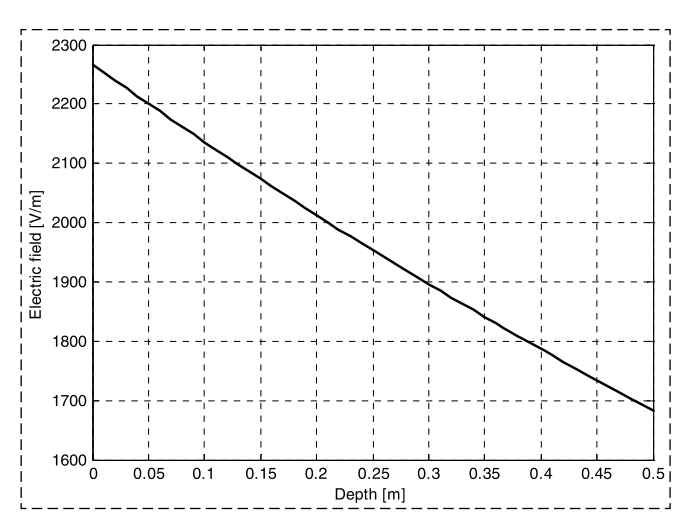


Fig. 2.2. Electric field (without mine)

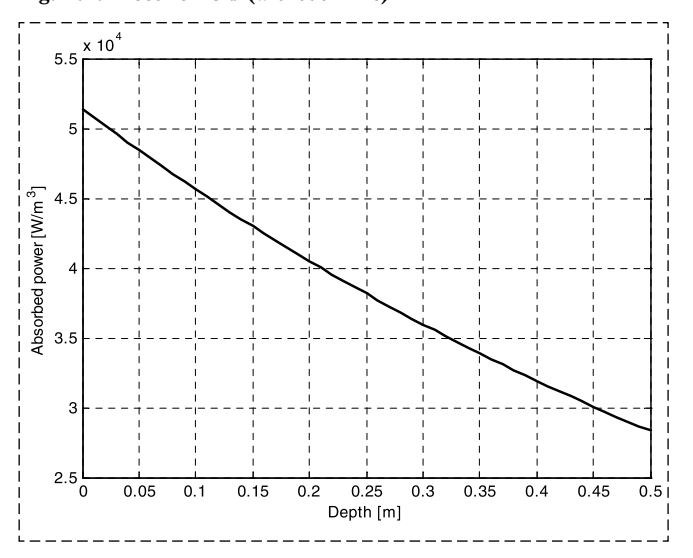


Fig. 2.3 Absorbed power (without mine)

the power absorbed by the soil and by the landmine [15, 16]. A plastic landmine with  $\varepsilon_r = 2.3$  and  $\tan(\delta) =$ =  $0.66 \cdot 10^{-4}$  was considered. It is assumed that the microwaves do not suffer attenuation while passing through the mines, since these are constituted, in its bigger part, by plastic material. The model includes a value for the dielectric constant of the ground. In general case, the ground is an anisotropic medium whose properties are changed with the frequency, moisture content and temperature. The model contains the following parameters: f = 2.45 GHz, common frequency of microwave heating systems,  $P_t =$ = 1000 W, power emitted by the microwave klystron,  $depth = 0.5 \text{ m}, \ \epsilon_r = 10, \text{ typical relative permittivity}$ for sand,  $\sigma = 10$  mS/m, idem,  $\theta_i = 65^\circ$ . The reflection coefficient of 0.1649 and the optimal incidence angle of 72° were used in the model.

The following graphics (Fig. 2.2—2.5) show the electrical field and absorbed power without the

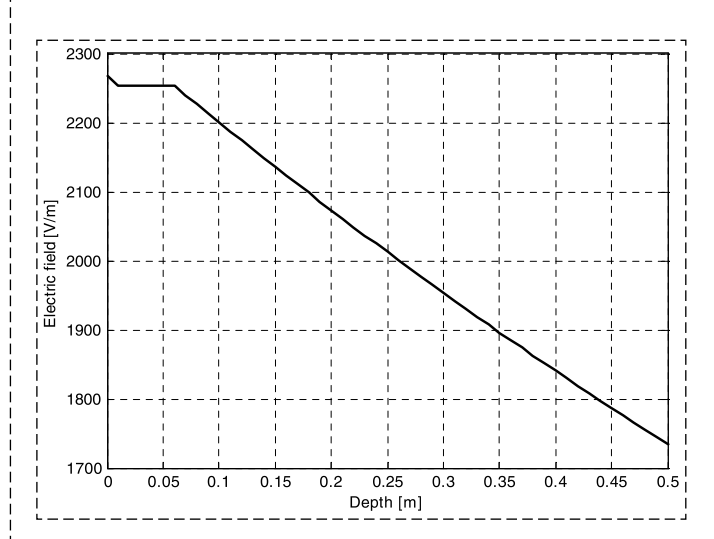


Fig. 2.4. Electric field (with mine)

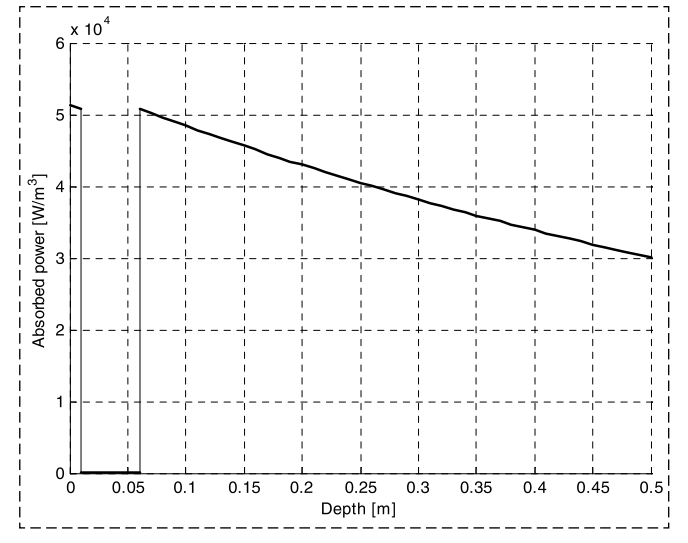


Fig. 2.5. Absorbed power (with mine)

mine and with the mine of 5 cm height, as a function of depth.

An analysis of the graphics shows that the electric field does not suffer attenuation through the mine and, therefore, the mine absorbs almost no power. The heat transfer has a central role in electric heating applications. A heat transfer process can occur by conduction, convection or radiation. By the application of electric heating, all these mechanisms are important and can actuate independently or in combination. According to the Fourier law, the rate of heat transfer from one body to another body at a different temperature can be expressed by the following equation

$$q = -Ak\frac{dT}{dx},\tag{2.11}$$

where k is the thermal conductivity, dT/dx is the thermal gradient in the heat flux direction and A is the heat flux cross-sectional area.

The equation for convection heat transfer phenomena is

$$q = Ah_{\tau}(T_s - T_{\infty}), \tag{2.12}$$

where  $h_{\tau}$  is the heat transfer coefficient and A is the characteristic area,  $T_s$  is the surface temperature,  $T_{\infty}$  is the atmospheric temperature. The heat transfer coefficient is a complex value that depends on the specific heat, viscosity, thermal conductivity, density, and temperature difference.

Radiation represents the main heating process by electromagnetic energy. The heat exchange between two gray surfaces,  $A_1$  and  $A_2$ , can be expressed by Stefan-Boltzmann law,

$$q_R = F(\varepsilon_1, \varepsilon_2, A_1, A_2)\sigma(T_1^4 - T_2^4),$$
 (2.13)

where  $\sigma$  is the Stefan-Boltzmann constant and  $F(\varepsilon_1, \varepsilon_2, A_1, A_2)$  is a view factor that considers the system geometry, particularly the relative orientation of areas  $A_1$  and  $A_2$ . The parameter  $\varepsilon$  represents the material emissivity.

By the energy conservation law, the energy flowing into a surface,  $\Pi_{t}$ , plus the internal heat generation, Pv, should equal the energy stored in the surface,  $\Pi_{\sigma}$ , plus the energy abandoning the surface,  $\Pi_{\epsilon}$ :

$$\prod_{1} + Pv = \prod_{\sigma} + \prod_{\varepsilon} . \tag{2.14}$$

The internal heat generation in a material is a process that can be provoked by the Joule effect with the flow of an electrical current, or by dielectric heating with microwaves. Dielectric heating occurs when a

substance is exposed to an electromagnetic field with frequencies between 10 and 10<sup>5</sup> MHz, corresponding to wavelengths from 30 m to 3 µm respectively.

The heating rate of material exposed to microwaves (dielectric heating) can be calculated by the energy conservation law, supposing the inexistence of boundary losses by radiation or convection:

$$\rho_0 c \frac{dT}{dx} = Pv \Rightarrow \frac{dT}{dx} = \frac{\omega E^2 \epsilon \tan \delta}{c \rho_0}, \quad (2.15)$$

where c is the specific heat and  $\rho_0$  is the material density. The rate of a temperature variation is expressed in terms of conductivity or heat loss, electric field and operating frequency. This equation is a good approximation of the temperature variation inside the material, since the thermal conductivity can be neglected in this case.

The general equation for mass and heat transfer, particularly in non-homogeneous materials is very complex. The general equation for heat transfer, including the term of convection and the volumetric source of heat  $P_{\nu}$  can be written as

$$c\rho_0 \left( \frac{\partial T}{\partial t} + \upsilon \nabla T \right) = -\nabla q + Pv,$$
 (2.15)

where T is the temperature, q is the vector of total heat flux,  $\rho_0$  is the material density and  $\upsilon$  is the speed vector for the heat transfer fluid. The term  $\nabla(p\upsilon)$  relative to compressible fluids at a pressure p was ignored in the above equation. If the material is submitted to radiation, then the heat flux q should include the radiation term  $(q_R)$  and the conduction term  $q_c$ :

$$q = q_c + q_R = -k_e \nabla T + q_R,$$
 (2.16)

where  $k_e$  is the effective thermal conductivity. Replacing the equation (2.16) in the equation (2.15) we obtain

$$c\rho_0 \frac{\partial T}{\partial t} = \nabla (k_e \nabla T) - c\rho_0 \upsilon \nabla T - \nabla q_R + Pv.$$
 (2.17)

The volumetric heating can be a consequence of ohmic heating by an electric current flow in the material, surface currents generated by induction heating, or reorientation of electric dipoles due to dielectric heating.

The modelling of a volume heating by microwave radiation can be done using the Partial Differential Equations (PDE) toolbox of Matlab. This toolbox provides a graphical interface that allows modelling the shape and properties of the materials to be studied.

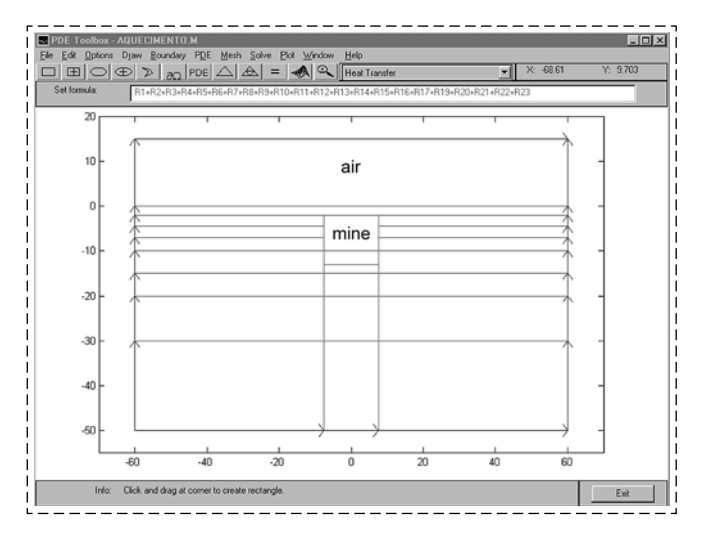


Fig. 2.6. Definition of the problem boundary

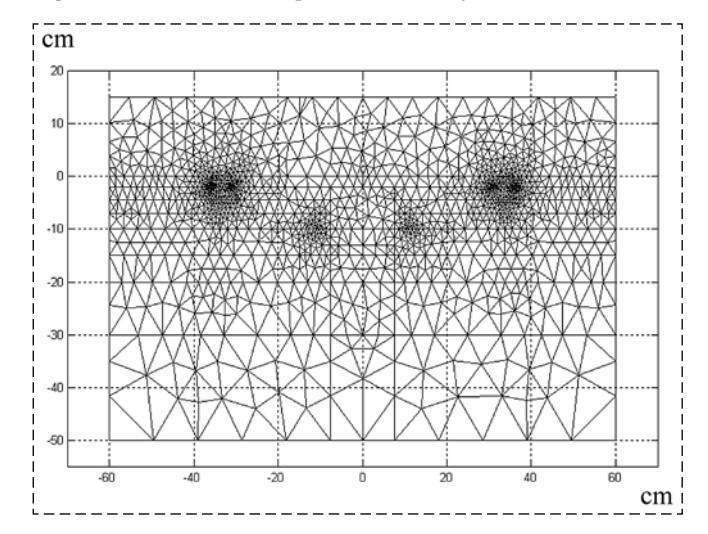


Fig. 2.7. Mesh of triangular finite elements

The following equation was calculated over the mesh of finite elements generated by the toolbox:

$$\rho_0 c \frac{\partial T}{\partial t} - \nabla (k \nabla T) = P v + h (T_{ext} - T), \quad (2.18)$$

where  $\rho_0$  is the material density, c is the specific heat, T is the temperature,  $T_{ext}$  is the external temperature, t is the conduction coefficient, t represents the source of heat and t is the heat transfer coefficient by convection.

This example considers the absorbed power equal to power released by the source of heat. The first step to simulate the soil heating is to draw the geometry of the problem boundaries using the toolbox graphical interface.

In Fig. 2.6, the model representation of the soil, a mine and the surrounding air can be seen.

The next step is to specify the boundary conditions. The Dirichlet type of boundary conditions allows specifying the temperature in the boundary.

After specifying the boundary conditions, it is necessary to specify the parameters for each type of material. To finish the modelling, it is necessary to generate a mesh of triangular finite elements. The mesh can be automatically generated by the PDE toolbox (see Fig. 2.7), but it can be adjusted manually.

The zones with higher temperature variation have finer mesh (mine and surface areas) in order to model the process accurately. The mesh of triangular finite elements is used for calculations of the heat distribution in the soil containing a mine.

Fig. 2.8 shows the temperature distribution inside a volume of soil containing a plastic mine in the interior after exposing the workspace with microwaves. The simulation initial temperature of 290 °K was considered for all the materials.

The simulation is composed of two phases. In the first phase, the workspace is exposed to homogeneous electromagnetic radiation. The temperature raises according to the materials properties.

The initial values of the second phase are the final values of the first phase. In this phase the material is not exposed to radiation, so only diffusion phenomena's occur by heat conduction. As it can be seen in Fig. 2.9, the surface over the mine is colder

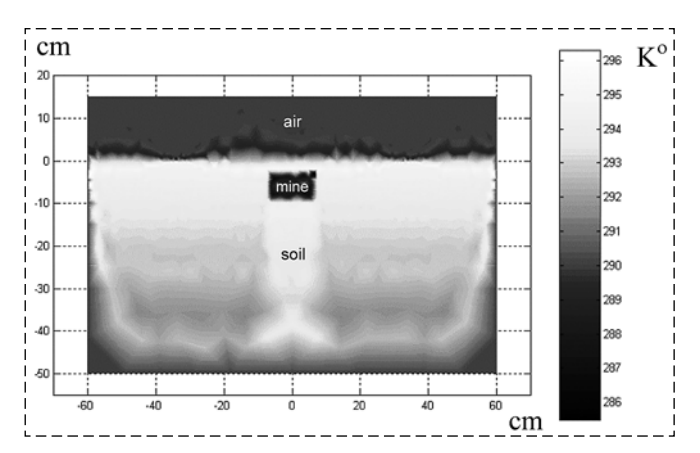


Fig. 2.8. Heat distribution after the first phase

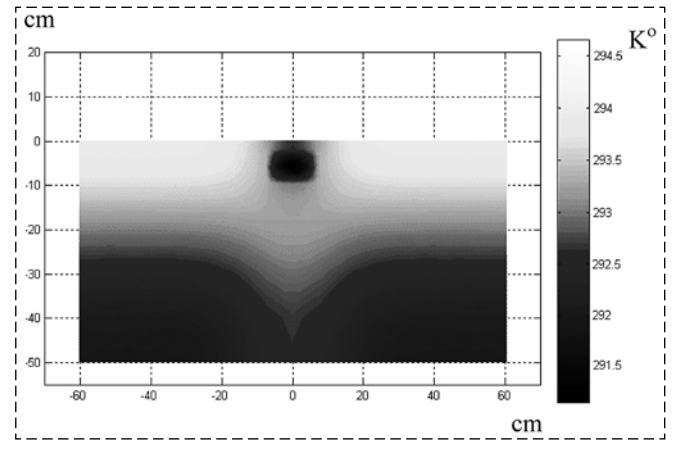


Fig. 2.9. Heat distribution in the end of second phase

than the neighborhood because the quantity of heat accumulated over the landmine is smaller than in the other regions, leading to faster cooling.

As a result, a signal about the mine position is generated by the detector. The control unit uses this signal to identify a mine angle position relative to the manipulator end-effector and gives a control signal to the manipulator drive for positioning of the neutralizator above the detected mine.

## 3. Manipulator drive modelling

A diagram of the drive control unit is shown in Fig. 3.1. The observer is placed in the control loop to minimize the number of sensors for the control.

A diagram of the manipulator drive is presented in Fig. 3.2.

The manipulator of a length L and an end-effector with the technological load (detection block and neutralizator) of mass m, is actuated by doubleacting pneumatic power cylinders by means a gear with a lever d. The considered drive system with pressure variation in pneumatic power cylinders [7] is described by non-linear differential equations of the third order

$$\ddot{\varphi} = p \frac{2F_n l}{mL^2} - f(\dot{\varphi});$$

$$\dot{p} = -\frac{2PF_n l}{V} \dot{\varphi} + \frac{RT}{V} g,$$
(3.1)

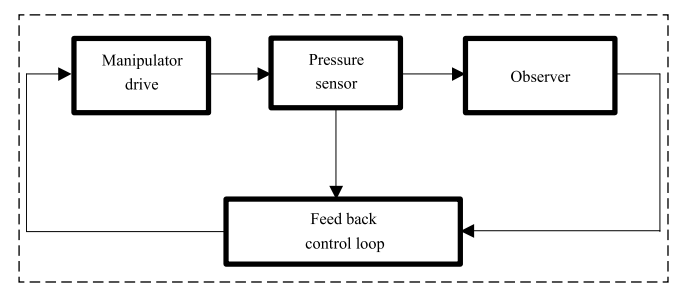


Fig. 3.1. Diagram of the drive control unit

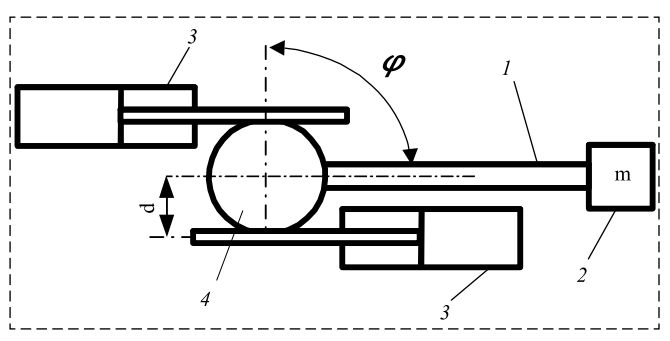


Fig. 3.2. Manipulator drive: 1 - manipulator; 2 - technological load; 3 - cylinders; 4 - gear

where  $\varphi$  is the angular position of the manipulator gripper, p is the current pressure difference in pneumatic cylinder volumes,  $F_n$  is the cross section of the cylinder piston, d is a lever of the acting force, R is the gas constant, T is the absolute temperature of working gas, V is the full volume of the pneumatic cylinder, P is the pressure inside the cylinder chambers in an equilibrium position of the cylinder pistons, g is the molar gas consumption in the pneumatic cylinder chambers,  $f(\dot{\varphi})$  is the summand taking into account the friction force of the drive system.

The force of inertia for rather large values of mass m considerably exceeds the friction force in the drive system. In this case, it is possible to transform the system (3.1) as follows

$$\dot{x}_1 = a_{13}x_3;$$
 $\dot{x}_2 = x_1;$ 
 $\dot{x}_3 = -a_{31}x_1 + u,$ 
(3.2)

where

$$x_1 = \dot{\varphi}; x_2 = \varphi; x_3 = p;$$
  
 $a_{13} = \frac{2F_n d}{mL^2}; a_{31} = \frac{2PF_n d}{V}; u = \frac{RT}{V}g.$  (3.3)

Thus, the phase coordinates of the system are the angular position, the angular velocity of the manipulator end-effector, and the pressure in pneumatic power cylinders. The control parameter is gas consumption. The problem of minimization of the positioning coordinates of the system (3.2) and, simultaneously, of the control energy consumption should be solved. It is possible to solve the task by means of the following quadratic criterion

$$I = \int_{0}^{\infty} (r_2 x_2^2 + r_3 x_3^2 + \rho u^2) dt, \qquad (3.4)$$

where  $r_2$ ,  $r_3$ ,  $\rho$  are adjustable coefficients. The control of the system is carried out by means of a gas flow valve. Information about the current system state is obtained from the pressure sensor, connected with the pneumatic cylinders, and from the observer [17].

The following moving object is considered:

$$\dot{x}(t) = A(t)x(t) + B(t)u(t);$$
 (3.5)

$$y(t) = C(t)x(t), \tag{3.6}$$

where x is an unknown n vector of the object state, u is a known control p vector, y is a vector of measured output parameters, A, B, C are given matrixes of corresponding dimensions.

To determine the state vector of an observed *n* system with linearly independent *m* outputs, it is enough

to have an n-m observer. Let us consider a (n-m) n matrix D with independent constant row elements using the matrix C. If a vector z is a result of transforming of the state vector x(t) by the matrix D, then

$$\begin{bmatrix} y(t) \\ z(t) \end{bmatrix} = \begin{bmatrix} C \\ D \end{bmatrix} x(t).$$
 (3.7)

The observation problem can be resolved if it is possible to obtain an estimation  $\hat{z}$  of the vector z, and that an error  $\tilde{z} = z - \hat{z}$  tends to zero. Let us suppose that a variation of the estimation is described as:

$$\frac{d}{dt}\hat{z} = F\hat{z}(t) + Gu(t) + Hy(t). \tag{3.8}$$

To study the time behavior of the error  $\hat{z}$  it is possible to use the following differential equation:

$$\frac{d}{dt}\tilde{z}(t) = \frac{d}{dt}(z - \hat{z}) = D\dot{x}(t) - \frac{d}{dt}\hat{z}(t).$$

Replacing the derivatives according to differential equations (3.1) and (3.4), we obtain

$$\frac{d}{dt}\tilde{z}(t) = DAx - F\hat{z} + (DB - G)u - Hy.$$

Substituting here  $\hat{z} = Dx - \tilde{z}$  and y = Cx, we have:

$$\frac{d}{dt}\tilde{z}(t) = F\tilde{z}(t) + (DA - FD - HC)x(t) + (DB - G)u(t).$$

It means that the error  $\hat{z}$  tends to zero irrespective of x and u, if the matrixes in the equation (3.8) are chosen as follows:

$$F$$
 — asymptotically stable,  
 $G = DB$ ; (3.9)  
 $DA - FD = HC$ . (3.10)

It then results in:

$$\frac{d}{dt}\tilde{z}(t) = F\tilde{z}(t).$$

Therefore,

$$\tilde{z}(t) = \exp(Ft)\tilde{z}(0)$$

or

$$\hat{z}(t) = Dx(t) - \exp(Ft)\tilde{z}(0).$$

The function  $\tilde{z}(t)$  can be used as an approximation for z(t) in the equation (3.3). Now the synthesis of

the observer is reduced to a solution of the equation (3.10) with additional limitations about the stability of the matrix F and the mutual lines independence of the matrixes D and C. The indicated solution exists if the matrixes A and F have different eigenvalues [18].

Defining:

$$\dot{x} = \begin{bmatrix} \dot{x}_1 \\ \dot{x}_2 \\ \dot{x}_3 \end{bmatrix}; x = \begin{bmatrix} x_1 \\ x_2 \\ x_3 \end{bmatrix}; A = \begin{bmatrix} 0 & 0 & a_{13} \\ 1 & 0 & 0 \\ -a_{31} & 0 & 0 \end{bmatrix}; B = \begin{bmatrix} 0 \\ 0 \\ 1 \end{bmatrix} (3.11)$$

it is possible to record the system (3.2) in a matrix form

$$\dot{X} = AX + BU. \tag{3.12}$$

Taking into account, that for the considered case

$$C = [0 \quad 0 \quad 1], \tag{3.13}$$

and accepting:

$$H = \begin{bmatrix} 1 \\ 1 \end{bmatrix}; F = \begin{bmatrix} -1 & 0 \\ -2 & 0 \end{bmatrix}; D = \begin{bmatrix} d_{21} & d_{22} & d_{23} \\ d_{31} & d_{32} & d_{33} \end{bmatrix}$$
(3.14)

we can obtain equations for the observer. The equation (3.7), taking into account (3.13) and (3.14), can be written as:

$$\begin{bmatrix} y \\ \hat{z}_1 \\ \hat{z}_2 \end{bmatrix} = \begin{bmatrix} 0 & 0 & 1 \\ d_{21} & d_{22} & d_{23} \\ d_{31} & d_{32} & d_{33} \end{bmatrix} \begin{bmatrix} \hat{x}_1 \\ \hat{x}_2 \\ x_3 \end{bmatrix}$$
(3.15)

and the equation (3.10) can be presented as:

$$\begin{bmatrix} d_{21} & d_{22} & d_{23} \\ d_{31} & d_{32} & d_{33} \end{bmatrix} \begin{bmatrix} 0 & 0 & a_{13} \\ 1 & 0 & 0 \\ -a_{31} & 0 & 0 \end{bmatrix} +$$

$$+ \begin{bmatrix} 1 & 0 \\ 2 & 0 \end{bmatrix} \begin{bmatrix} d_{21} & d_{22} & d_{23} \\ d_{31} & d_{32} & d_{33} \end{bmatrix} = \begin{bmatrix} 1 \\ 1 \end{bmatrix} \begin{bmatrix} 0 & 0 & 1 \end{bmatrix}.$$
(3.16)

From (3.16) we have the following equation system:

$$d_{22} - a_{31}d_{23} + d_{21} = 0;$$

$$d_{32} - a_{31}d_{33} + 2d_{21} = 0;$$

$$d_{22} = 0;$$

$$a_{13}d_{21} + d_{23} = 1;$$

$$a_{13}d_{31} + 2d_{23} = 1.$$
(3.17)

It is possible now to determine the elements of the matrix D from the system (3.17) as:

$$D = \begin{bmatrix} a_{31}(1+a_{13}a_{31})^{-1} & 0 & (1+a_{13}a_{31})^{-1} \\ a_{13}^{-1} \left[1-2(1+a_{13}a_{31})^{-1}\right] & -2a_{31}(1+a_{13}a_{31})^{-1} & 0 \end{bmatrix}.$$
 (3.18)

According to the equation (3.9), we have:

$$G = \begin{bmatrix} \left(1 + a_{13}a_{31}\right)^{-1} \\ 0 \end{bmatrix}. \tag{3.19}$$

Taking into account equations (3.14) and (3.19), it is possible to present (3.8) as:

$$\begin{bmatrix}
\hat{z}_{1} \\
\hat{z}_{2}
\end{bmatrix} = \begin{bmatrix}
-1 & 0 \\
-2 & 0
\end{bmatrix} \begin{bmatrix}
\hat{z}_{1} \\
\hat{z}_{2}
\end{bmatrix} + \\
+ \begin{bmatrix}
(1 + a_{13}a_{31})^{-1} \\
0
\end{bmatrix} U(t) + \begin{bmatrix}
1 \\
1
\end{bmatrix} y(t)$$
(3.20)

or

$$\dot{\hat{z}}_1 = -\hat{z}_1 + (1 + a_{13}a_{31})^{-1}u + y; 
\dot{\hat{z}}_2 = -2\hat{z}_2 + y.$$
(3.21)

According to the equation (3.15) and determining  $k = (1 + a_{13}a_{31})$ , we have:

$$y = x_3;$$

$$\hat{x}_1 = a_{31}^{-1} k^{-1} \hat{z}_1 - a_{31}^{-1} x_3;$$

$$\hat{x}_2 = -\frac{1}{2} a_{31}^{-1} k \hat{z}_2 + \frac{1}{2} a_{31}^{-1} a_{13}^{-1} (k-2) \hat{x}_1.$$
(3.22)

The obtained observer is described by equations (3.21) and (3.22).

Thus, measuring the variable  $x_3 = p$  and receiving by an observer output the variables  $\hat{x}_1 = \hat{\phi}$  and  $\hat{x}_2 = \hat{\phi}$ , we have necessary information to design a feedback control system of the pneumatic manipulator by the criterion (3.4).

An implementation of the observer model according to equations (3.21) and (3.22) is shown in Fig. 3.3.

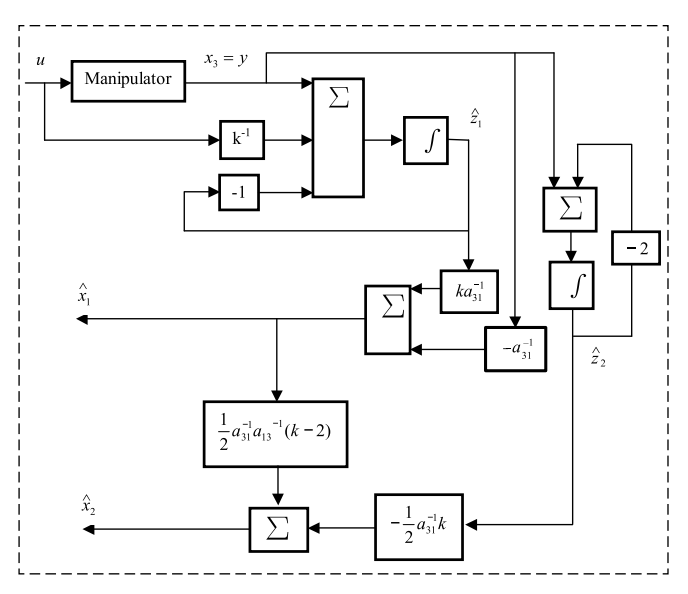


Fig. 3.3. Implementation of the observer model

The implementation of the observer demands two integrators, four summators and seven scaling blocks. The observer output gives the necessary information for the synthesis of the control system.

For the considered stationary system we can use the equation [19]:

$$R_1 - PBR_2^{-1}B'P + AP + PA = 0 (3.23)$$

where the matrixes A and B are determined according to the equations (3.11), and:

$$R_{1} = \begin{bmatrix} 0 & 0 & 0 \\ 0 & r_{2} & 0 \\ 0 & 0 & r_{3} \end{bmatrix}; R_{2} = \rho; P = \begin{bmatrix} P_{11} & P_{12} & P_{13} \\ P_{21} & P_{22} & P_{23} \\ P_{31} & P_{32} & P_{33} \end{bmatrix}. (3.24)$$

An optimal control of the system (3.2), (3.4) can be written as follows:

$$u_o = -R_2^{-1}B'PX = -\rho^{-1}(P_{31}x_1 + P_{32}x_2 + P_{33}x_3),$$
 (3.25)

where the elements i = 1, 2, 3 are amplifying coefficients in the feedback loop of the control system.

The problem of the optimal control is reduced to the determination of necessary elements of the matrix P, which can be obtained from the equation (3.23). For such a purpose a solution algorithm of the equation (3.23) for stationary systems with infinite time of observation can be used.

Let us introduce the following matrix:

$$R = \begin{bmatrix} -A & BR_2^{-1}B' \\ R_1 & A' \end{bmatrix}, \tag{3.26}$$

and an expression for a matrix

$$\lambda I - R \tag{3.27}$$

where I is the identity matrix,  $\lambda$  is an eigenvalue of the matrix (3.4). A determinant of the matrix (3.27) is:

$$\det(\lambda I - R) = \lambda^3 \left( \lambda^3 - \lambda \frac{r_3}{\rho} + \lambda a_{13} a_{31} \right) +$$

$$+ \lambda a_{13} a_{31} (\lambda^3 + \lambda a_{13} a_{31}) + \frac{a_{13}}{\rho} (-r_2 a_{13}).$$

Considering:

$$\lambda^2 = \alpha \tag{3.28}$$

then, rewriting the expression for  $det(\lambda I - R)$  with usage of (3.28) and equating it to zero, we have:

$$\alpha^{3} + \alpha^{2} \left( a_{13} a_{31} - \frac{r_{3}}{\rho} \right) + \alpha^{2} a_{13} a_{31} +$$

$$+ \alpha (a_{13} a_{31})^{2} - \frac{a_{13}}{\rho} r_{2} a_{13} = 0.$$
(3.29)

It is possible to solve the equation (3.29) using equations (3.3) and defining  $\lambda_1$ ,  $\lambda_2$ ,  $\lambda_3$  that are located to the left of an imaginary axis. We can introduce the determinant of the matrix (3.27) as:

$$\det(\lambda I - R) = (-1)^n \Delta(\lambda) \Delta(-\lambda), \qquad (3.30)$$

where  $\Delta(\lambda)$  — scalar polynomial of power *n*. Thus,

$$\Delta(\lambda) = (\lambda - \lambda_1)(\lambda - \lambda_2)(\lambda - \lambda_3). \tag{3.31}$$

Substituting values  $\lambda_1$ ,  $\lambda_2$ ,  $\lambda_3$  in the equation (3.31), we can obtain a numerical value for  $\Delta(\lambda)$ . Then, making a substitution  $\lambda$  and R, we form a matrix

$$\Delta(R) = \begin{bmatrix} R_1 & R_2 \\ R_3 & R_4 \end{bmatrix}. \tag{3.32}$$

The matrix R is defined by the equation (3.4) and is equal to

$$R = \begin{bmatrix} 0 & 0 & -a_{31} & 0 & 0 & 0 \\ -1 & 0 & 0 & 0 & 0 & 0 \\ a_{31} & 0 & 0 & 0 & 0 & \rho^{-1} \\ 0 & 0 & 0 & 0 & 1 & -a_{31} \\ 0 & r_2 & 0 & 0 & 0 & 0 \\ 0 & 0 & r_3 & a_{13} & 0 & 0 \end{bmatrix}.$$
(3.33)

Now it is possible to have values  $R_2$  and  $R_4$  from equations (3.32) and (3.33). According to [17],

$$P = R_4 R_2^{-1}. (3.34)$$

The necessary elements of the matrix P are defined from the equation (3.34). Using them in the equation (3.3), we obtain the optimal control solution as:

$$u_o = -\rho^{-1}(P_{31}\dot{\varphi} - P_{32}\varphi - P_{33}p).$$
 (3. 35)

The system using the optimal control (3.35) is asymptotically stable.

An implementation of the optimal control (3.35) with a simulation of the object (3.2) is shown in Fig. 3.4.

Thus, the implementation of the optimal control demands only three scaling blocks and one summator. The simulation of the object consists of two integrators, one summator and two scaling blocks. The control signal is used in the drive for the optimal positioning of the manipulator.

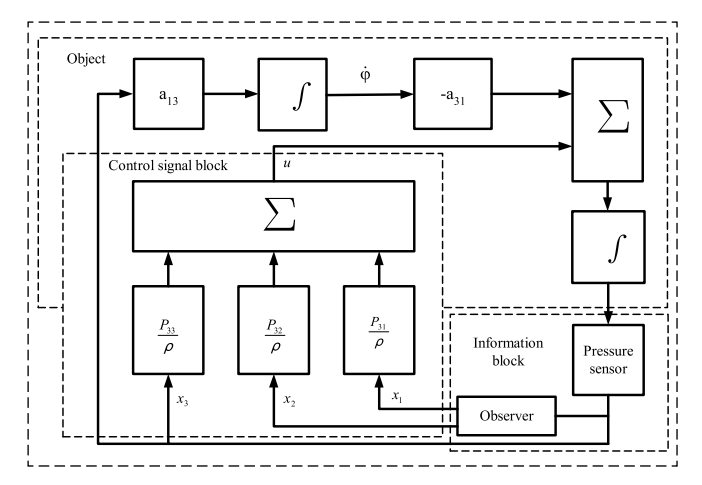


Fig. 3.4. Implementation of the optimal control modelling

The simulation and an experimental test with the industrial pneumatic manipulator Tsyklon [7] with the following numerical parameters:  $P = 60 \text{ N/cm}^2$ , d = 8 cm, m = 200 N, L = 80 cm,  $F_n = 133 \text{ cm}^2$ ,  $V = 2790 \text{ cm}^3$ ,  $r_2 = 10$ ,  $r_3 = 1$ ,  $\rho = 28$  were done. For these parameters, the optimal control solution according to (3.35) is

$$u_o = 1,249 \cdot 10^5 \dot{\varphi} - 1,130 \cdot 10^5 \varphi - 11,06 \cdot 10^5 p.$$
 (3.36)

Simulation and experimental results for the  $30^{\circ}$  angle positioning (Fig. 3.5, a) and  $90^{\circ}$  angle positioning (Fig. 3.5, b) show that end-effector trajectories tend to the set angle exponentially quickly.

An accuracy difference between modelling trajectories and experimental trajectories is inside 15 %. This difference is caused by the friction influence in the pneumatic elements of the real manipulator. The accuracy discrepancy decreases by increasing of the rotation angle value. Therefore, the modelling assumptions correspond in a satisfactory manner to the real positioning process parameters.

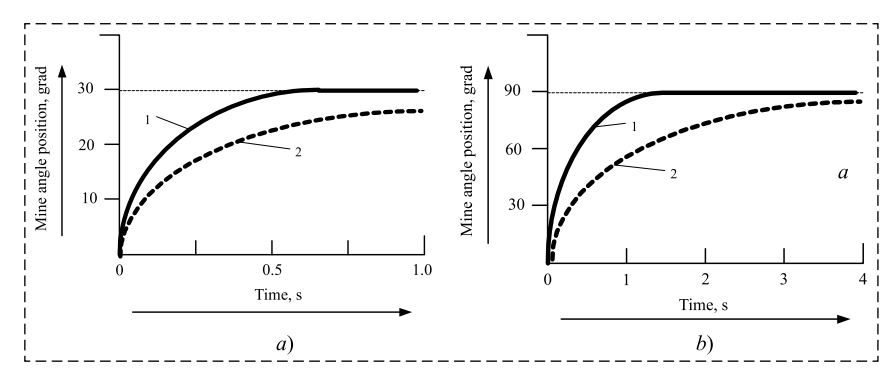


Fig. 3.5. Simulation results of manipulator positioning:  $a-30^\circ$  angle positioning;  $b-90^\circ$  angle positioning (I- modelling trajectory; 2- experimental trajectory)

The described modelling method can be applied to manipulators with other design parameters for the double-acting pneumatic drive.

#### **Conclusions**

Modelling of the demining manipulator is an important task while developing demining robots, in order to estimate the design and the dynamic parameters of the detection block and the manipulator drive unit. This methodology appears well suited to achieve the effective functioning of the automatic demining system.

The IR detector functioning is modelled in the mine searching two-phase mode. The obtained temperature distribution inside a volume of soil containing a plastic mine after exposing the workspace with microwaves, permits generating information about the location of the mine. This information is used as an input signal for modelling of the position control of the mine neutralizator by means of the double-acting pneumatic manipulator drive.

The problem of the optimal manipulator positioning in the sense of the control energy consumption minimization is solved. The feedback loop contains only one sensor to perform the optimal positioning of the third-order control object due to an observer application. Simulation results with numerical design parameters of the industrial pneumatic manipulator show that end-effector trajectories tend to the set angle exponentially quickly.

The comparison of the modelling and of the experimental results shows that the modelling assumptions are well adapted to the real process and that the proposed technique provides effectiveness in the system operation.

#### References

- 1. **Landmine** Monitor 2015, International Campaign to Ban Landmines Cluster Munition Coalition (ICBL-CMC), 2015.
- 2. **de Almeida A. T., Khatib O. K.** Autonomous Robotics Systems, Springer, 1998.
  - 3. Mikulic D. Design of demining machines, Springer, 2013.
- 4. **de Santos P. G., Cobano J. A., Garcia E., Estremera J., Armada M.** A six-legged robot-based system for humanitarian demining missions, *Mechatronics*, 2007, vol. 17, no. 8, pp. 417–430.
- 5. **Santana P. F., Barata J., Correia L.** Sustainable robots for humanitarian demining, *International Journal of Advanced Robotic Systems*, 2007, vol. 4, no. 2, pp. 207—218.
- 6. **Rachkov M., Marques L., de Almeida A. T.** Automation of Demining, University Press, University of Coimbra, 2002.
- 7. Rachkov M. Yu., Crisóstomo M., Marques L., de Almeida A. T. Positional control of pneumatic manipulators for construction tasks, Automation in Construction, Elsevier Science, 2002, 11 (6), pp. 655—665.
- 8. **Yinon J.** Forensic and environmental detection of explosives, Wiley, 1999.
- 9. **Noro D., Sousa N., Marques L., de Almeida A. T.** Active Detection of Antipersonnel Landmines by Infrared, Annals of Electrotechnical Engineering Technology, Portuguese Engineering Society, 1999.
- 10. **Pozar D. M.** Microwave Engineering, Second Edition, John Wiley & Sons, 1998.
- 11. **Griffiths J.** Radio Wave Propagation and Antenas: an introduction, Prentice-Hall, 1987.
- 12. **Bengtsson N. E., Ohlsson T.** Microwave Heating in the Food Industry, *Proc. of the IEEE*, 1974, vol. 62, no. 1.
- 13. **Metaxas A. C.** Foundations of Electroheat a unified approach, John Wiley & Sons, 1996.
- 14. MATLAB, High-Performance Numeric Computation and Visualization Software, The Math Works, Inc., 2016.
- 15. **Hipp J. E.** Soil Electromagnetic Parameters as Functions of Frequency, Soil Density, and Soil Moisture, *Proc. of the IEEE*, 1974, vol. 62, no. 1.
- 16. Hallikainen M. T. et al. Microwave Dielectric Behavior of Wet Soil Part I: Empirical Models and Experimental Observations, *IEEE Transactions on Geoscience and Remote Sensing*, 1985, vol. GE-23, no. 1.
- 17. **Luenberger D.** Observers for multivariable systems, *IEEE Trans. on Automatic Control*, AC-11, 1966.
- 18. **Brammer K., Ziffling G.** Kalman-Bucy filter, Nauka, Moscow, 1982 (in Russian).
- 19. **Reutenberg Ya. N.** Automatic control, Nauka, Moscow, 1978 (in Russian).